iScience

Article

MERS-CoV spike vaccine-induced N-terminal domain-specific antibodies are more protective than receptor binding domain-specific antibodies

Graphical abstract

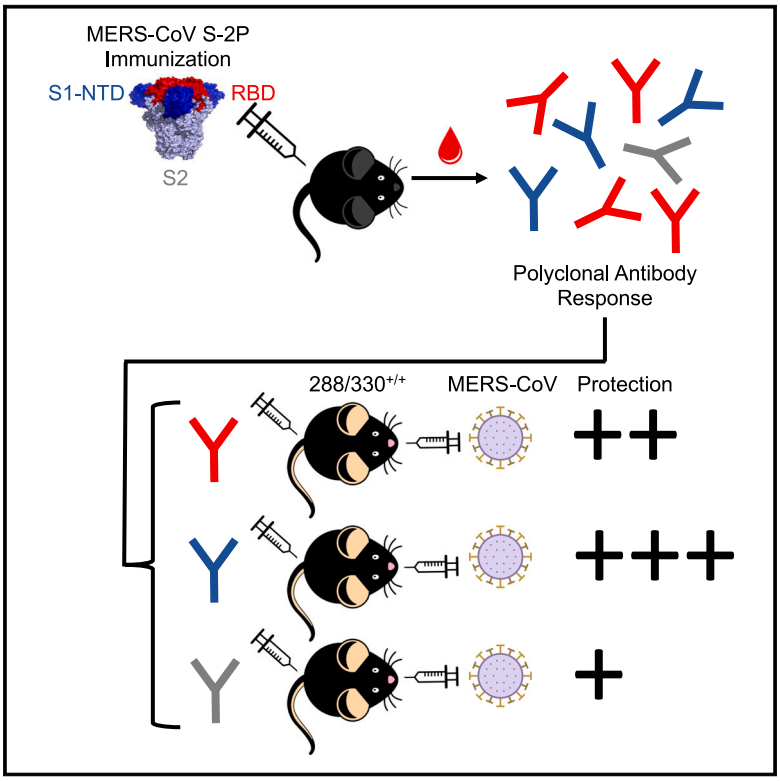

Authors

Olubukola M. Abiona, Nianshuang Wang, Sarah R. Leist, ..., Jason S. McLellan, Barney S. Graham, Kizzmekia S. Corbett-Helaire

Correspondence

kizzmekia_corbett@hsph.harvard.edu

In brief

Immunology; Immunity; Virology

Highlights

- Prefusion MERS-CoV spike vaccination elicits antibodies to diverse antigenic sites
- Vaccination with prefusion MERS-CoV spike ΔRBD protects mice against challenge
- Non-RBD antibodies elicited by MERS-CoV spike are more protective than RBD antibodies
- Neutralization by non-RBD antibodies is most consistent in plaque-reduction assays

Abiona et al., 2025, iScience *28*, 111632
February 21, 2025
https://doi.org/10.1016/j.isci.2024.111632

CellPress

iScience

CellPress
OPEN ACCESS

Article

MERS-CoV spike vaccine-induced N-terminal domain-specific antibodies are more protective than receptor binding domain-specific antibodies

Olubukola M. Abiona,[1,10] Nianshuang Wang,[2,10] Sarah R. Leist,[3,10] Alexandra Schäfer,[3] Adam S. Cockrell,[3] Lingshu Wang,[1] Sandhya Bangaru,[4] Laura Stevens,[5] Rachel L. Graham,[3] Jacob F. Kocher,[3] Yaroslav Tsybovsky,[6] Masaru Kanekiyo,[1] Azad Kumar,[1] Kaitlyn M. Morabito,[1] Osnat Rosen,[1] Wei Shi,[1] Anne Werner,[1] Yi Zhang,[1] Cynthia Ziwawo,[1] Christian K.O. Dzuvor,[7] Charis Palandjian,[7] Connor Eastman,[8] Hannah R. Matthews,[7] Jeswin Joseph,[7] James D. Chappell,[5] Wing-Pui Kong,[1] John R. Mascola,[1] Andrew B. Ward,[4] Mark R. Denison,[5] Ralph Baric,[3] Jason S. McLellan,[2] Barney S. Graham,[1] and Kizzmekia S. Corbett-Helaire[1,7,9,11,*]

[1]Vaccine Research Center, National Institutes of Allergy and Infectious Diseases, National Institutes of Health, Bethesda, MD 20892, USA
[2]Department of Molecular Biosciences, University of Texas at Austin, Austin, TX 78712, USA
[3]Department of Epidemiology, University of North Carolina at Chapel Hill, Chapel Hill, NC 27599, USA
[4]Department of Integrative Structural and Computational Biology, The Scripps Research Institute, La Jolla, CA 92037, USA
[5]Department of Pediatrics, Vanderbilt University Medical Center, Nashville, TN 37212, USA
[6]Electron Microscopy Laboratory, Cancer Research Technology Program, Frederick National Laboratory for Cancer Research Sponsored By the National Cancer Institute, Frederick, MD 21702, USA
[7]Department of Immunology and Infectious Diseases, Harvard T.H. Chan School of Public Health, Boston, MA 02115, USA
[8]Program in Virology, Harvard Medical School, Boston, MA 021115, USA
[9]Howard Hughes Medical Institute, Chevy Chase, MD 20815, USA
[10]These authors contributed equally
[11]Lead contact
*Correspondence: kizzmekia_corbett@hsph.harvard.edu
https://doi.org/10.1016/j.isci.2024.111632

SUMMARY

The COVID-19 pandemic underscores the need to prepare for future emerging coronavriuses (CoVs) by understanding the principles behind effective CoV vaccine design such as protective immunity and antibody responses. To study which epitopes and subdomains contribute to *in vivo* protection, we utilized the prefusion-stabilized spike protein of MERS-CoV, MERS S-2P, as a vaccine immunogen. Vaccination with MERS S-2P elicited both receptor-binding domain (RBD)- and non-RBD-specific antibodies, including N-terminal domain (NTD)-specific G2-and CDC2-A2-like antibodies. Intriguingly, the immunogen MERS S-2P_ΔRBD, MERS S-2P with the RBDs removed, protects comparably to S1 and S-2P immunogens against MERS-CoV challenge. Moreover, passive transfer studies of polyclonal IgG from MERS S-2P immunized mice depleted of subdomain-specific antibodies demonstrated that non-RBD antibodies protected more than non-NTD antibodies. Altogether, these findings illustrate that *in-vivo* protection is not solely driven by RBD-specific antibodies and highlights the importance of targeting non-RBD sites in future CoV vaccine designs.

INTRODUCTION

The 2019 zoonotic spillover of severe acute respiratory coronavirus 2 (SARS-CoV-2) represents the third coronavirus (CoV), along with SARS-CoV and Middle East respiratory syndrome coronavirus (MERS-CoV), to cause an outbreak over the last two decades. MERS-CoV, which has a 35% mortality rate, continues to cause steady state transmission in the Middle East, with the most recent outbreak occurring in May 2024. With proven pandemic potential and a large and expanding number of beta-CoVs being discovered in bats,[1] there is a high likelihood that additional CoVs will emerge.[2] Understanding the fundamental principles of protective immunity against CoVs is essential for vaccine design and preparing for the next CoV outbreak.

Since MERS-CoV emerged in 2012, it has been defined by regional containment with sporadic outbreaks. MERS-CoV outbreaks cause a high frequency of severe lower respiratory tract disease and high mortality[3,4]; thus MERS-CoV has been designated as a high-priority pathogen for vaccine development by the Coalition for Epidemic Preparedness Innovations and the World Health Organization. Multiple MERS-CoV vaccine candidates have been shown to elicit neutralizing antibodies (nAbs) and protect small animal and nonhuman primate models against challenge,[5–9] but despite initial enthusiasm, commercial interest in developing MERS-CoV vaccine candidates has

waned. There are currently no licensed prophylactic or therapeutic countermeasures, partly due to a lack of well-defined immunity and immune correlates of protection. Without clear immunogenicity targets, advanced product development is unlikely. Therefore, our study aimed to elucidate the role of antibody (Ab) specificity and function in protection against MERS-CoV infection.

The CoV spike (S) surface glycoprotein, a trimeric class I fusion protein on the virion surface, is the primary target of nAbs.[10–12] S is composed of S1 and S2 subunits; S1 forms a cap with two distinct structural subdomains of the N-terminal domain (NTD) and the receptor-binding domain (RBD). S2 contains the fusion machinery that mediates membrane fusion and viral entry.[13–15] High-resolution structural analysis of full-length prefusion S trimers from MERS-CoV and other CoVs has revealed several potential vulnerable antigenic sites of interest, including the RBD, NTD, quaternary surfaces, and S2 [16–20]. To gain a better understanding of the MERS-CoV S Ab epitope architecture, we and others have isolated and characterized monoclonal antibodies (mAbs) that recognize epitopes in each of the subdomains including RBD-, NTD-, and S2-specific binding classes.[5–9,21–24] RBD-specific mAbs primarily function by blocking S binding to its host-cellular receptor, dipeptidylpeptidase 4 (DPP4).[8,9,22,24,25] *In vitro* measurements of neutralizing activity suggest that RBD-specific mAbs are generally more potent than mAbs targeting other domains. However, when combined with mAbs against sites outside the RBD, the likelihood of viral escape decreases.[8,26] Non-RBD neutralizing mAbs exhibit diverse mechanisms of action, such as blocking DPP4 access,[27] inhibiting prefusion to post-fusion conformational changes in S,[26] and interfering with cell-cell or virus-to-cell fusion.[24] However, the role of Ab specificities in vaccine-induced polyclonal sera and protection against coronavirus diseases is ill-defined yet urgently needed for the development of effective vaccine strategies.[28–30]

Therefore, we explored the antigenic landscape of vaccine-induced immunity to MERS-CoV S-2P, a prefusion-stabilized MERS S vaccine antigen in this study. Our previous studies show that MERS S-2P elicits more potent neutralizing antibodies than S1 monomers[17]; these data led to the inclusion of 2P mutations in SARS-CoV-2 vaccines currently in use globally.[31–33] Since S1 monomers predominantly induce RBD-directed neutralizing Ab responses,[22] we hypothesized that MERS S-2P elicits a qualitatively different repertoire of Abs. Here, we show that vaccination with MERS S-2P elicits Abs targeting diverse sites, including RBD and non-RBD epitopes, like the NTD-specific G2-and CDC2-A2-like Abs. Passive transfer studies of polyclonal Ig isolated from S-2P-immunized mice depleted of RBD- or NTD-specific Abs demonstrated that non-RBD Abs had relatively more protective capacity compared with non-NTD Abs. These findings emphasize the importance of targeting vulnerable sites outside the RBD, not only to diminish the possibility of viral escape but also to improve protective efficacy. This knowledge will help guide future vaccine design efforts for MERS-CoV and potentially other coronaviruses using multiple S domains, particularly those that recognize relatively more conserved and protective epitopes.

RESULTS

Middle East respiratory syndrome coronavirus spike vaccination elicits antibodies to diverse antigenic sites

To examine Ab specificity and protection in the context of vaccination, we utilized our rationally designed prefusion-stabilized MERS-CoV S antigen, MERS S-2P.[17] In BALB/cJ mice, vaccination with S-2P trimers elicits more potent and broad nAbs than S1 monomers.[17] For S1 vaccination, nAb responses are primarily RBD-specific.[22] Thus, we hypothesized that S-2P elicits Abs to diverse epitopes, including non-RBD regions. To test this hypothesis, we designed a full-length stabilized MERS S-2P antigen that lacks RBD, designated "MERS S-2P_ΔRBD." To remove the immunodominant RBD (residues Gly380–Lys577) and redirect the immune responses to other more conserved regions of S, we inserted a short GSGG linker to connect Gly380 and Lys577, which are separated by only 8 Å (Figures S1A and S1B). Following expression and purification, gel-filtration chromatograms indicated that S-2P_ΔRBD achieved expression levels similar to S-2P, which was 30-fold higher than S-WT (Figure S1C).[17] As evidenced by negative-stain electron microscopy (EM), S-2P_ΔRBD also maintained a homogeneous prototypic prefusion morphology (Figure S1D). We next tested the ability of S-2P_ΔRBD to bind well-characterized neutralizing mAbs to confirm RBD removal and ensure proper antigenicity. S-2P_ΔRBD bound well to the NTD-specific mAb G2 and S2-specific mAb G4 but was unable to bind to the RBD-specific mAb D12, as expected (Figure S1E). Collectively, these data indicate that S-2P_ΔRBD lacks the RBD while maintaining the prefusion conformation of the S protein and the availability of other antigenic sites.

To dissect the specificity of Abs elicited by different vaccinations, we immunized C57BL/6J mice (n = 10/group) with S1, S-2P, and S-2P_ΔRBD at weeks 0 and 3. At week 6, we purified IgG from the pooled sera of each group using Protein G. Subsequently, we depleted the sera of antibodies with specificity to MERS S-2P, S1, NTD, and RBD, as well as to an irrelevant viral fusion protein (respiratory syncytial virus pre-F). Following depletion, we assessed the remaining serum Abs for binding IgG specific to S-2P (Figures 1A–1C), S1 (Figures S2A–S2C), NTD (Figures S2D–S2F), and RBD (Figures S2G–S2I) domains by ELISA. We also tested the sera for MERS-CoV M35c4 pseudovirus neutralization (Figures 1D–1F). Mock depleted sera revealed that S1 immunization elicited robust S-2P-specific binding Abs, amassing serum endpoint titers of 2.7×10^4 (Figures 1A–1C). S1- and S-2P-depleted serum from S1-immunized mice did not bind any of the proteins, confirming complete depletion (Figures 1A and S2). RBD depletion of S1-immune sera reduced binding to S-2P by ~20-fold and neutralization capacity by ~4-fold. In contrast, NTD depletion did not decrease the ability of S1-immune sera to bind S-2P or neutralize pseudoviruses, and mock-depleted S1-immune sera did not bind NTD suggesting that S1 immunization does not elicit NTD-directed Abs (Figures 1A, 1D, and S2D). These results indicate that S1 immunization elicits primarily RBD-specific Abs, recapitulating our previously published results.[22]

S-2P and S-2P_ΔRBD immunization elicited robust S-2P-specific binding Abs with endpoint titers of 8.3×10^4 and 1.9×10^4, respectively. Following S1 depletion, S-2P- and

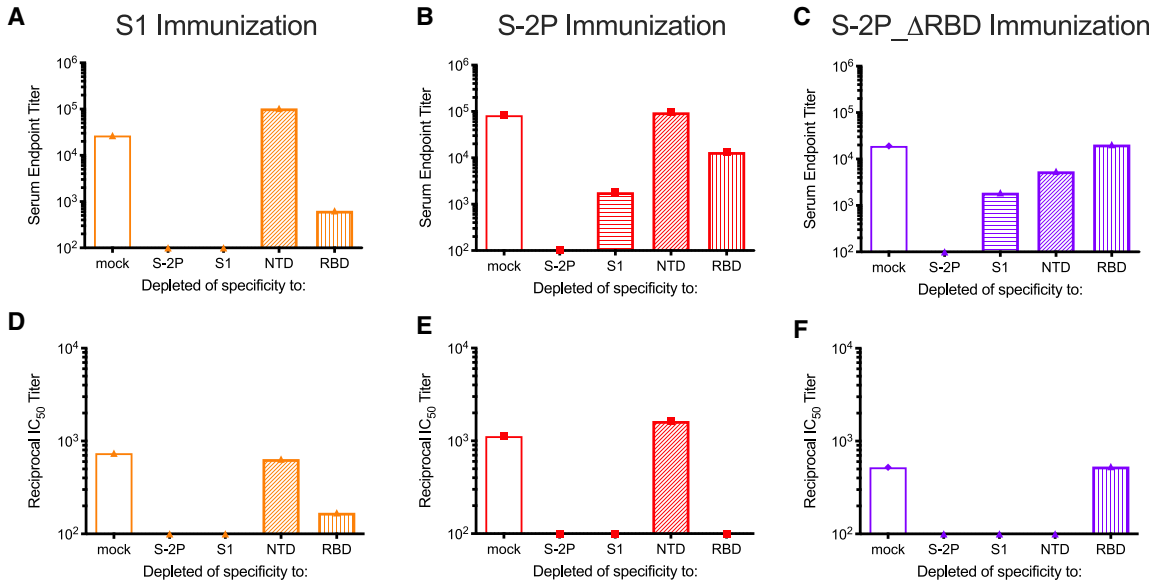

Figure 1. Dissection of MERS S domain-specific antibody responses

(A–F) Sera from MERS S1 (orange), S-2P (red), and S-2P_ΔRBD (purple) immunized mice (n = 10/group) were pooled and depleted of specificity to non-specific trimeric viral fusion protein (white), MERS S-2P (dots), MERS S1 (horizontal lines), MERS NTD (diagonal lines), or MERS RBD (vertical lines), respectively and assessed for (A-C) binding to MERS S-2P protein by fold-on-competed ELISA and (D-F) neutralizing antibodies against MERS M35c4 pseudovirus.

S-2P_ΔRBD-immune mouse sera retained 1.8 x 10^3 (~46-fold reduction) and 1.9 x 10^3 S-2P (~10-fold reduction) specific endpoint titers, respectively (Figures 1B and 1C). This suggests that both trimers elicit Abs specific to S surfaces that are not exposed on S1 monomers, including but not limited to the S2 domain and/or quaternary surfaces (Table S1). Consequently, S1 depletion resulted in the significant but not complete loss of pseudovirus neutralization. As expected, RBD depletion had no effect on the ability of S-2P_ΔRBD-immune sera to bind S-2P, as the immunogen lacks RBD. For those mice, NTD depletion left behind a serum endpoint titer of 5.4 x 10^3, representing a ~3.5-fold reduction (Figure 1C). These results serve to further confirm the presence of Abs specific to the S2 domain and/or quaternary surfaces. (Table S1). For S-2P-immune serum, the S-2P-specific binding capacity was similar after NTD depletion and largely remained following RBD depletion (1.3 x 10^4 serum endpoint titer) (Figure 1B). Mock-depleted S-2P-immune sera bound the NTD with an endpoint titer of 1.7 x 10^3, confirming the presence of NTD-specific Abs following S-2P vaccination (Figure S2E). For S-2P- and S-2P ΔRBD-immune sera, the majority of the pseudovirus neutralization titer was attributed to RBD- and NTD-specific Abs, respectively (Figures 1E and 1F). Together, these data show that S1 primarily elicits neutralizing Abs targeting the RBD, while S-2P immunization elicits Abs targeting the RBD, NTD, and other regions. Both RBD- and NTD-specific Abs contribute to neutralizing activity in polyclonal sera.

Middle East respiratory syndrome coronavirus spike trimers lacking receptor binding domains protect mice against challenge

Next, we assessed the protective capacity of polyclonal sera elicited through vaccination. To simultaneously assess protective Ab responses following MERS S1, S-2P, and S-2P_ΔRBD vaccination, we immunized 288/330$^{+/+}$ mice[34] with each antigen at 0 and 4 weeks. 288/330+/+ mice are genetically modified via CRISPR–Cas9 gene editing on the C57/BL6 backbone to encode two amino acids (positions 288 and 330) that match the human DPP4 sequence. The resulting 288/300$^{+/+}$ modification renders the mice susceptible to MERS-CoV replication whereby M35c4 is a serially passaged mouse-adapted MERS-CoV strain that replicates efficiently within the lungs and causes decreased survival, weight loss, decreased pulmonary function, and gross lung discoloration. Importantly, this lethal MERS-CoV mouse model has isolated viral replication in the lung as opposed to systemic viral replication.[34] Of interest for these studies, 288/330$^{+/+}$ are immune competent.[35] At 4 weeks post-boost, we challenged the immunized 288/330$^{+/+}$ mice with MERS-CoV M35c4. Each mouse received 0.02 μg of protein, which is 5-fold lower than the previously studied doses of S1 and S-2P.[17,22] Despite such a low dose, S1- and S-2P-immunized mice mounted neutralization IC_{50} titers of ~10^2 and ~10^3, respectively, against the MERS-CoVm35c4 pseudovirus. S-2P elicited a more potent neutralizing Ab response than S-2P_ΔRBD; in fact, 5 out of 15 S-2P_ΔRBD-immunized mice had undetectable (IC_{50} > 1:40) levels of neutralizing Abs (Figure 2A). Surprisingly, all S-2P_ΔRBD-immunized mice, including those with undetectable neutralizing Ab levels, were protected from weight loss and mortality following the challenge. Similarly, S1- and S-2P-immunized mice did not suffer from weight loss following the challenge (Figure 2B). All three immunogens were effective at preventing lung discoloration (Figures 2C and 2D), decreasing airway obstruction (PenH) (Figures S3A–S3B), and increasing lung air flow

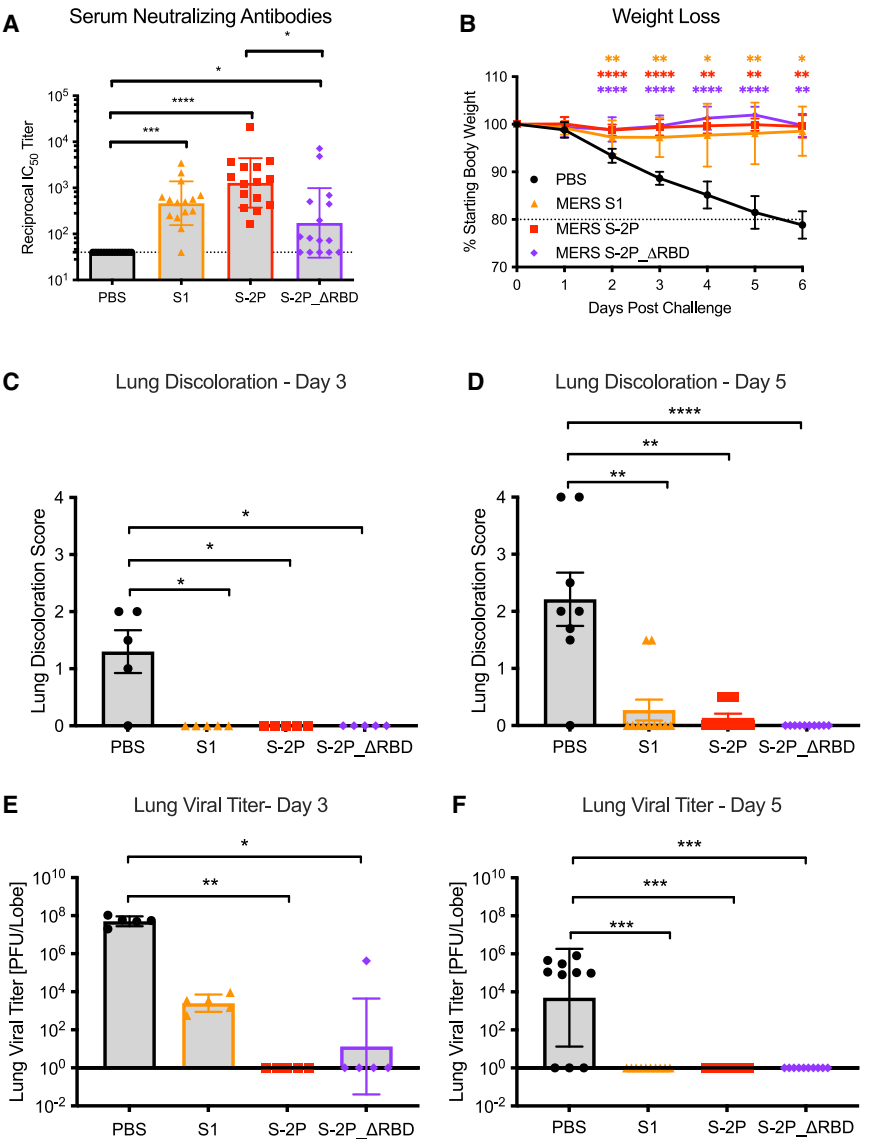

Figure 2. Ability of prefusion-stabilized MERS S trimers to protect mice from lethal challenge

(A–F) 288/330$^{+/+}$ mice were immunized at week(s) 0 and 3 with PBS (black), MERS S1 (orange), MERS S-2P (red), or MERS S-2P_ΔRBD (purple) and challenged 4 weeks post-boost with a lethal dose of MERS-CoV. Experimental groups were compared by 1-way ANOVA with the Kruskal–Wallis post-test. * = p-value <0.05, ** = p-value <0.01, *** = p-value <0.001, **** = p-value <0.0001.

(A) Pre-challenge sera were collected from a subset of mice and assessed for neutralizing antibodies against MERS m35c4 pseudovirus. The dotted line represents the assay limit of detection. Each symbol represents an individual mouse. Bars represent the geometric mean titer (GMT) of each group.

(B) Following challenge, mice were monitored for weight loss. The mean of each group is represented by symbols. Error bars represent SEMs. The dotted line represents the threshold of weight loss at which mice were sacrificed.

(C–F) At days 3 (C,E) and 5 (D,F) post-challenge, a subset of mouse lungs was harvested for analysis of (C-D) congestion score (0 = no discoloration, 4 = 100% discoloration in all lobes) and (E-F) viral titers. Each symbol represents an individual mouse. Bars represent the (C-D) mean or (E-F) GMT of each group. Error bars represent (C-D) SEMs or (E-F) geometric standard deviations (SDs).

(EF50) (Figures S3C–S3D), compared to PBS. On day 3 post-challenge, lungs from MERS S1-immunized mice contained ~10^3 plaque-forming units (PFU)/lobe of MERS-CoV (Figure 2E). While the virus was cleared by day 5 (Figure 2F), these results suggest that Abs elicited by MERS S1, which mainly target the RBD, may only partially prevent viral infection when neutralizing activity is undetectable. In contrast, S-2P and S-2P_ΔRBD-immunized mice were completely protected from lung viral replication (Figures 2E and 2F). Removal of RBD from S-2P did not impede the ability of the trimer to protect mice against challenge, despite lower levels of neutralizing Abs. These results suggest that each immunogen may render protection via different Ab subsets or antibody-mediated mechanisms as seen in other reports and demonstrate that potently neutralizing RBD-directed Abs are not necessary for vaccine-induced MERS-CoV protection.[36–39]

Middle East respiratory syndrome coronavirus spike vaccine-induced non-receptor-binding domain polyclonal antibodies are more protective than polyclonal antibodies targeting the receptor-binding domain despite lower neutralization potency

To further understand the protective capacity of Abs of different specificities, we assessed the ability of domain-depleted IgGs from MERS S-2P immune sera to protect mice against the MERS-CoV challenge. We strategically titrated mock-depleted IgG in C57BL/6J mice to target a steady-state IC_{50} titer of 10^2 in the m35c4 pseudovirus assay following passive transfer. Subsequently, we chose a 0.5 mg dose of domain-depleted IgG to administer intraperitoneally into each 288/330$^{+/+}$ mouse. A subset of mice was bled 1 h pre-challenge for analyses of humoral immunity, and the remaining mice were challenged with MERS-CoV m35c4 (Figure S4B). As expected, mice immunized with S-2P-depleted IgG succumbed to infection, suffering from severe weight loss (Figure 3A), high levels of lung discoloration (Figures 3B and 3C), and ~10^8 PFU/lung lobe viral titers (Figure 3D). Conversely, mock-depleted IgG fully protected mice from weight loss (Figure 3A) and lung hemorrhage discoloration (Figures 3B and 3C). On day 3 post-challenge, mice immunized with mock-depleted IgG showed significantly decreased lung viral

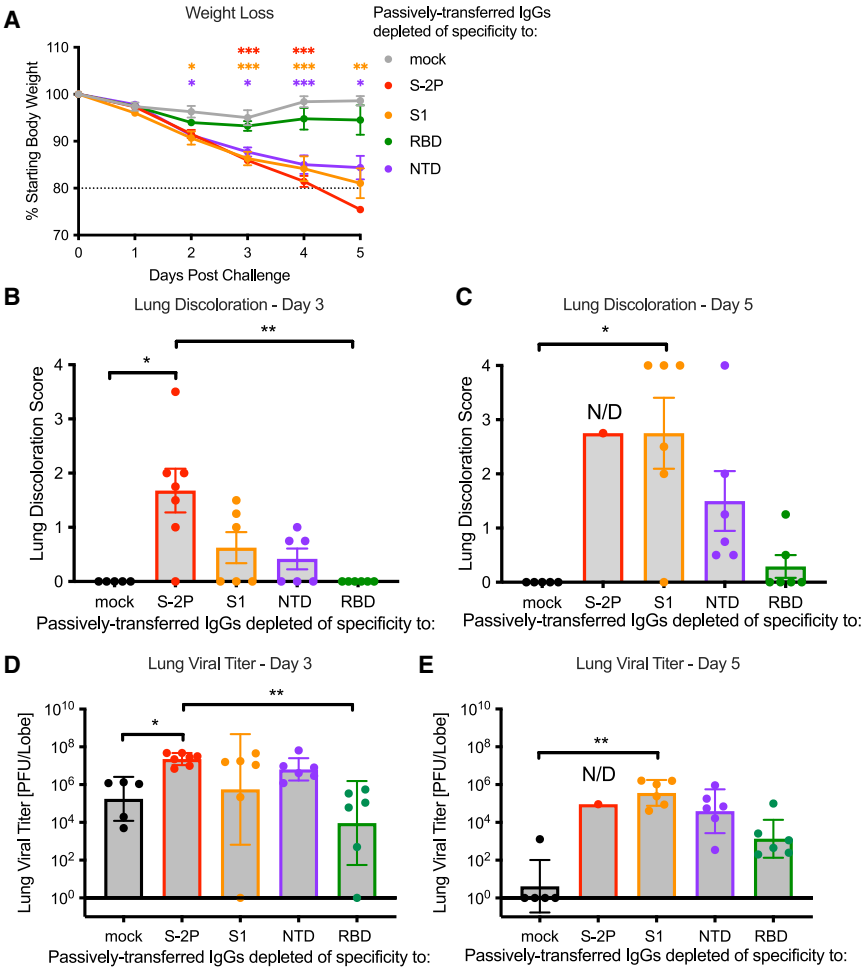

Figure 3. Ability of MERS S domain-specific IgGs to protect mice from lethal challenge

(A–E) IgGs were purified from MERS S-2P immunized wild-type mice, depleted of specificity to non-specific trimeric viral fusion protein (black), MERS S-2P (red), MERS S1 (orange), MERS NTD (purple), or MERS RBD (green) and passively transferred to 288/330$^{+/+}$ mice. At 24 h post-immunization, mice were challenged with a lethal dose of MERS-CoV m35c4.

(A) Following challenge, mice were monitored for weight loss. The mean of each group is represented by symbols. Error bars represent SEMs. The dotted line represents the threshold of weight loss at which mice were sacrificed. Experimental groups were compared to the mock-depleted group by 1-way ANOVA with the Kruskal–Wallis post-test. * = p-value <0.05, ** = p-value <0.01, *** = p-value <0.001. Weight loss curves were completed in two separate experiments with similar results.

(B–E) At 3 and 5 days post-challenge, a subset of mouse lungs was harvested for analysis of (B-C) congestion score (0 = no discoloration, 4 = 100% discoloration in all lobes) and (D-E) viral titer. Each symbol represents an individual mouse. Bars represent the (B-C) mean or (D-E) GMT of each group. Error bars represent (B-C) SEMs or (D-E) geometric SDs. Groups were compared by 1-way ANOVA with the Kruskal–Wallis post-test. * = p-value <0.05, ** = p-value <0.01.

replication, and by day 5, their lungs were clear of MERS-CoV (Figures 3D and 3E). Mice immunized with S1-depleted IgG, which removes NTD and RBD-specific Abs but retains IgG specific to S2, quaternary surfaces, and other regions (Table S1), lost significant weight in comparison to mice immunized with mock-depleted IgG (Figure 3A). The high levels of lung hemorrhage and viral discoloration suggest that S1-depleted IgGs were ineffective in preventing MERS-CoV replication in the lung (Figures 3B–3E). Surprisingly, mice immunized with NTD-depleted IgG, which retains Abs to the RBD-specific and other domains (Table S1; Figure S5), showed significant weight loss (Figure 3A) and ~10^7 PFU/lobe lung lobe viral titers (Figures 3D and 3E). In contrast, RBD-depleted IgG, which retains NTD-specific G2-and CDC2-A2-like Abs (Figure 4, Data S1), protected mice from severe weight loss (Figure 3A). Additionally, mice passively transferred with RBD-depleted IgG had significantly less lung discoloration and lung viral replication mice that received S-2P-depleted IgG (Figures 3B–3E). These results indicate that vaccine-induced polyclonal Abs (pAb) targeting regions outside the RBD, particularly those targeting the NTD, are more protective than pAbs specific to the RBD under these conditions.

Non-receptor-binding domain antibodies elicited by Middle East respiratory syndrome coronavirus spike vaccination contain two major N-terminal domain-binding classes

Next, we defined S-2P-induced NTD-specific Ab subsets by performing electron microscopy-based polyclonal epitope mapping (EMPEM). Our previous work revealed the presence of at least three distinct NTD-specific Ab classes.[8] The most potent neutralizing binding class is exemplified by the murine mAb G2 and nonhuman primate mAb JC57-13, which exhibit MERS-CoV EMC pseudovirus IC_{50} neutralization titers of 0.01 μg/mL and 0.07 μg/mL, respectively. The human mAbs CDC2-A2 and CDC2-A10 represent individual binding classes with lower IC_{50} titers of 0.45 μg/mL and 0.18 μg/mL, respectively.[8] To understand S-2P-induced Ab populations, we isolated, dissected, and characterized IgG from S-2P-vaccinated mice. C57BL/6J mice (n = 300) were immunized at weeks 0 and 3 with 1 μg of S-2P adjuvanted with Sigma Adjuvant System, an oil-in-water emulsion. At 2-, 4-, and 6-week post-boost, we isolated IgG from pooled sera and subsequently depleted the IgG of specificity to the RSV pre-F (mock), MERS S-2P, S1, NTD, and RBD, yielding domain-depleted IgG for subsequent experiments (Figures S4A and S5). We visualized Fabs digested from RBD-depleted polyclonal IgG bound to MERS S-2P by negative-stain EMPEM (Figure 4, Data S1). RBD-depleted (Figure 4, Data S1) and undepleted (Figure S6A) polyclonal Fabs contained Abs that bound the bottom of S-2P.

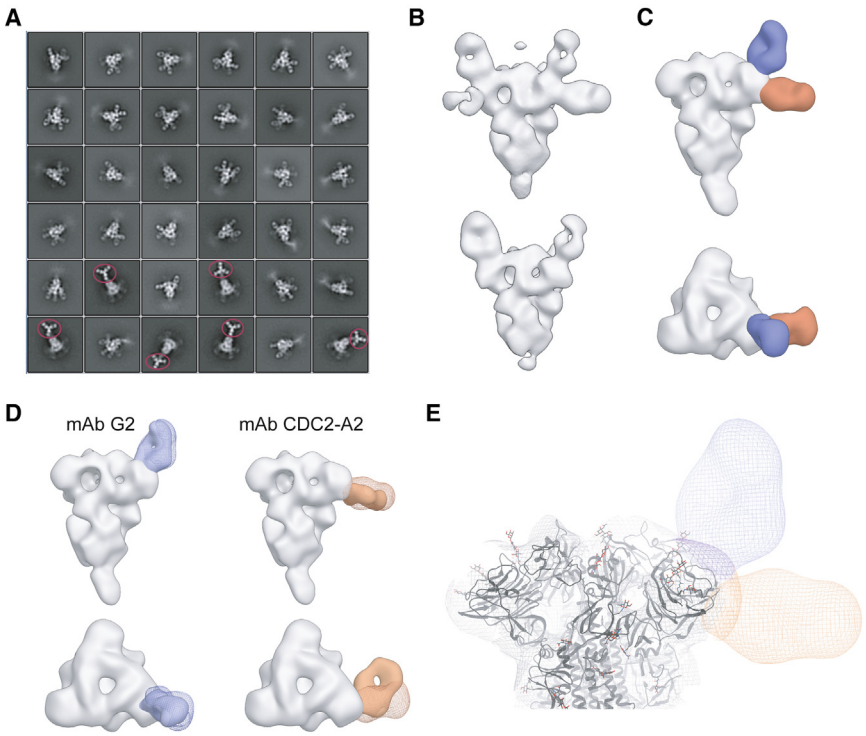

Figure 4. MERS S-2P trimer vaccination elicits G2-and CDC-A2-like NTD-specific Abs

(A) Representative 2D class averages from negative-stain EM analysis of MERS S-2P complexed with Fabs digested from RBD-depleted serum polyclonal IgGs.

(B) Refined 3D reconstructions from negative-stain EM analysis of MERS S-2P complexed with Fabs digested from RBD-depleted serum polyclonal IgGs.

(C) Side and top view of a composite 3D figure demonstrating the two NTD Fab specificities in purple and orange.

(D) Side and top views of composite 3D figures comparing each NTD specificity from polyclonal analysis (shown as mesh) to monoclonal antibodies G2 (solid purple) or CDC2-A2 (solid orange).

(E) Mesh representation of the composite figure shown in (C) with MERS spike structure (PDB# 5X5F) docked into the density for epitope depiction.

However, mock-depleted Fabs also contained these Abs, suggesting specificity to the foldon trimerization domain, which is located on the C-terminus of the S-2P and RSV pre-F constructs (Figure S6B). We were unable to visualize any S2-specific or quaternary Abs by this method, supporting the notion that S1-specific Abs are most abundant following S-2P vaccination. Interestingly, RBD-depleted Fabs contained two primary NTD-specific Ab populations (Figure 4, Data S1). One Fab class bound S-2P from a top angle; the other Fab class approached S-2P from the side. Overlaying densities of RBD-depleted Fabs with published structures of G2 bound to S-2P[27] revealed the top-binding Ab fractions to be akin to G2. Similarly, the side-binding RBD-depleted Ab fractions directly overlapped with the Fabs of the CDC2-A2 class of mAbs (Figures 4 and S6C–S6D and Data S1). Together, the polyclonal structures suggest either limited to no presence of CDC2-A10-like Abs[40] and that MERS S-2P vaccination elicits NTD-specific Abs that are predominantly G2/JC7-13-like and CDC2-A2-like.

We collected sera from similarly immunized 288/330$^{+/+}$ mice 11 h post-immunization (analogous to 1 h pre-challenge) to quantify circulating binding and neutralizing Abs. Mice passively transferred with 0.2 mg/kg of RBD-specific CDC2-C2 and NTD-specific G2 had similar amounts of circulating binding IgG at that timepoint (i.e., 2.6 μg/mL and 2.8 μg/mL, respectively). At the 1 mg/kg protective dose, mice immunized with CDC2-C2 had a 10-fold higher amount of circulating Abs (32.9 μg/mL) than mice immunized with 0.2 mg/kg (2.5 μg/mL) ($p < 0.01$). For G2-immunized mice, we observed a non-significant decrease in the amount of circulating Abs at the 1 mg/kg (9.96 μg/mL) compared to the 0.2 mg/kg dose (3 μg/mL). (Figure 5C). Mice immunized with 0.2 mg/kg of CDC2-C2 and G2 had similar geometric mean serum IC_{50} pseudovirus neutralization titers (37.1 and 20.6, respectively). Interestingly, mice that received 1 mg/kg of G2 with a neutralizing activity IC_{50} titer of 29.5 were protected, whereas mice that received 0.2 mg/kg of CDC2-C2 with a similar level of neutralizing activity (IC_{50} titer = 37.1) were not protected (Figures 5A, 5B, and 5D). These data suggest that while RBD specific CDC2-C2-like Abs possess potent *in vitro* pseudovirus neutralization activity, a larger quantity is required to confer *in vivo* protection compared to less potent neutralizing NTD-specific Abs such as G2. Moreover, these findings indicate that *in vitro* MERS-CoV pseudovirus neutralization may not always correlate with protection.

Plaque reduction neutralization tests uncovers neutralization activity of Middle East respiratory syndrome coronavirus spike vaccine-induced polyclonal non-receptor-binding domain antibodies

We next aimed to dissect the impressive protection conferred by vaccine-induced non-RBD IgG against the MERS-CoV challenge utilizing *in vitro* Ab analyses. Taking pre-challenge serum, from the above-mentioned passive transfer study, we first assessed the binding antibody capacity to MERS S-2P via ELISA. Mice that received S-2P- or S1-depleted IgG did not have any detectable MERS S-2P-specific serum binding Abs (>1:50 serum endpoint titer). Mice that were passively immunized with mock-, NTD-, or RBD-depleted IgG had modest (2.0–3.0 x 10^2) serum endpoint titers. We detected no significant difference between the groups, suggesting that the ability of non-RBD IgG to protect *in vivo* is not merely determined by their ability to bind recombinant MERS S trimer protein (Figure S8). To assess neutralization, we implemented two assays in cells: pseudovirus neutralization, using luciferase reporter lentiviruses expressing MERS-CoV EMC S in Huh 7.5 cells, and PRNT, using native MERS-CoV EMC in the Vero81 cell line. We tested the capacity of domain-depleted

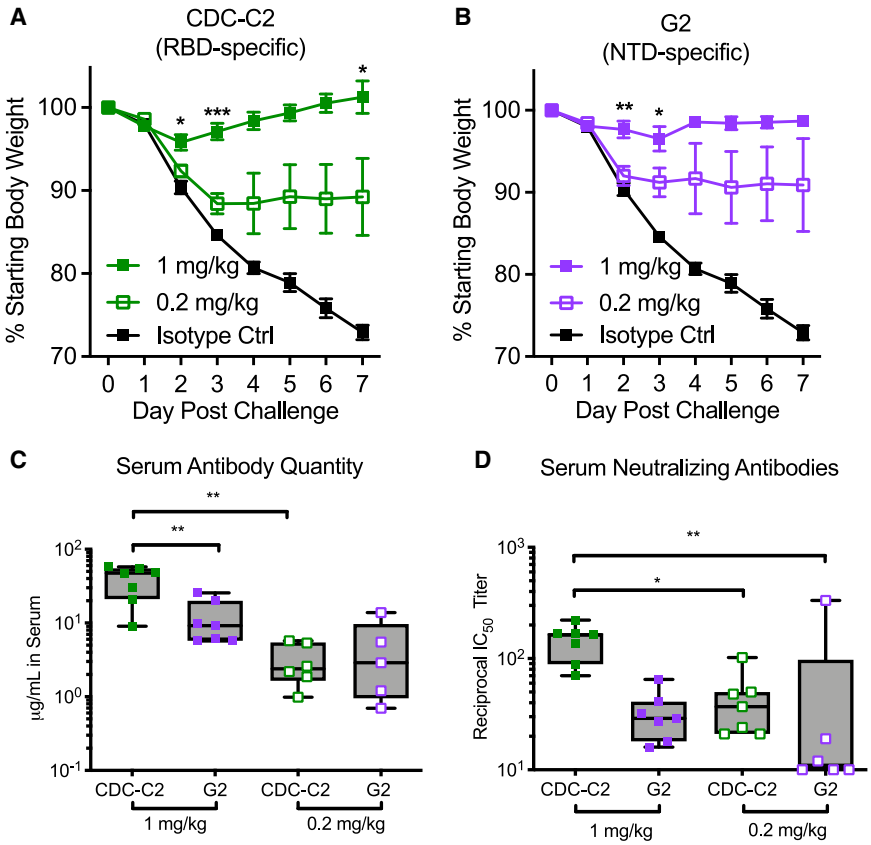

Figure 5. Protective antibody thresholds of RBD- and NTD-specific mAbs

(A and B) 288/330$^{+/+}$ mice were passively immunized with 1 mg/kg (closed squares) or 0.2 mg/mg (open squares) of RBD-specific mAb, CDC-C2 (green), G2 (purple), or an isotype control (black). At 12 h post-immunization, mice were challenged with a lethal dose of MERS-CoV m35c4. Following challenge, mice were monitored for weight loss. The mean of each group is represented by symbols. Error bars represent standard errors of the mean (SEMs). Doses were compared by 1-way ANOVA with the Kruskal–Wallis post-test. * = p-value <0.05, *** = p-value <0.001.

(C and D) 288/330$^{+/+}$ mice were bled 11 h following immunization and serum was assessed for the (C) quantity of MERS S-2P-specific binding antibodies or (D) reciprocal IC_{50} titer of serum neutralizing antibodies. Each symbol represents an individual mouse. Box represents the interquartile range and whiskers depict minimum and maximum. Groups were compared by the Mann–Whitney t-test. * = p-value <0.05, ** = p-value <0.01.

IgG to neutralize pseudovirus and found that NTD- and RBD-depleted IgG carried a similar neutralization capacity, with IC_{50} values of ~4 µg/mL (Table S2). In the PRNT assay, mock-depleted IgG and RBD-depleted IgG exhibited similar neutralizing activity and were about 3-fold more potently neutralizing than NTD-depleted IgG, although this difference was subtle (Table S2). We then assessed levels of circulating neutralizing Abs in mouse sera from 1 h pre-challenge. the serum neutralizing Ab titer ratio in mice that received RBD-depleted IgG (reciprocal IC_{50} = 62.6) to mock-depleted IgG (reciprocal IC_{50} = 69.9) group remained ~1:1 after challenge by PRNT assay (Table 1 and S2). Sera from mice that received RBD-depleted IgG had 4.5-fold more neutralizing activity than sera from mice that received NTD-depleted IgG (reciprocal IC_{50} = 13.8) (Table 1). Sera from mice immunized with S1-depleted IgG did not neutralize MERS-CoV by PRNT (reciprocal IC_{50} < 6) (Table 1), suggesting that any Abs present that are specific to S1 subdomains, S2, and/or quaternary surfaces do not play a pronounced role in neutralization. Thus, RBD- and NTD-specific Abs are mostly responsible for the PRNT neutralization differences observed by NTD- and RBD-depleted IgG, respectively. The ability to exclusively capture these differences by PRNT, but not by pseudovirus neutralization, may suggest that NTD-specific pAbs possess fundamentally different neutralization mechanisms than RBD-specific pAbs, which may correlate with increased protective efficacy. Together, our findings illuminate the importance of targeting vulnerable sites outside the RBD in MERS-CoV vaccines to improve protective efficacy.

DISCUSSION

The diverse array of countermeasures forged from the COVID-19 pandemic underscores the importance of defining mechanisms of immunity and correlates of protection. Unlike SARS-CoV-2, MERS-CoV has no licensed therapeutics or vaccines despite its designated as a top 10 priority pathogen by the World Health Organization.[41] By studying MERS-CoV, we can better facilitate the design and advancement of candidate vaccines for this virus and future emerging CoVs. In this report, we utilized a prefusion-stabilized MERS S vaccine antigen MERS S-2P[17] and subdomain variants to dissect vaccine-induced polyclonal site-specific Ab responses and to determine which specificities contribute to *in vivo* protection. While RBD-specific Abs are immunodominant and elicit potent *in vitro* neutralization of pseudoviruses, Abs that bind outside the RBD, particularly NTD-specific Abs, were more protective *in vivo*, despite similar levels of neutralizing activity measured in pseudotyped lentivirus reporter assays. In support of earlier work, our data demonstrates the importance of sites outside the RBD for protection and challenges the paradigm of current CoV vaccine strategies reliant on RBD-only immunogens and responses for protection.

Whereas neutralization following low-dose immunization with S-2P was attributed to RBD-specific Abs, S-2P elicited the binding of Abs targeting several antigenic sites, including, but not limited to, the RBD, NTD, and other non-S1 regions. Immunization with an S-2P construct that lacks the RBD, S-2P_ΔRBD, elicited primarily NTD-specific neutralizing Ab responses. These findings suggest that the RBD is the immunodominant antigenic site presented by vaccination with full-length S protein and, without the RBD, immunodominance shifts toward S1 NTD. The regulation of immunodominance is not completely

Table 1. Neutralization titers in mice following passive transfer of MERS S domain-specific IgGs

Passively transferred IgGs depleted of specificity to	Reciprocal IC_{50} (Serum GMT)[a]		
	Pseudovirus Neutralization	PRNT[b]	
		Mean	SEM
Mock	48.8	69.9	12.1
S-2P	<10	<6	ND[c]
S1	<10	<6	ND[c]
NTD	12.5	13.9	1.8
RBD	13.8	62.6	6.2

[a]Strain: MERS-CoV EMC.
[b]mean and SEM based on two PRNT experimental trials with two randomly selected sera from each group.
[c]N/D = not determined.

understood but broadly defines how B-cells induce the prevalence of antibodies toward specific epitopes,[42] in this case likely due to RBD epitope accessibility. We confirmed immunodominance by assessing domain-depleted IgG from S-2P immunized mice. RBD-, NTD-, and S1-depleted IgG bound to S-2P by ELISA, which confirmed S-2P immunization elicits a small quantity of S2-specific Abs. However, we were only able to visually reveal NTD-specific Abs in RBD-depleted polyclonal IgG by EM. Most of the human MERS-CoV mAbs reported to date are RBD-specific, with few being NTD-specific and even fewer S2-specific mAbs.[10,40] This also reflects the immunodominant hierarchy of S seen following natural infection from MERS-CoV and SARS-CoV-2, respectively[43,44]

From our studies, we found only two major binding classes of NTD-specific Abs, G2/JC57-13-like and CDC2-A2-like, which is surprising given the vast surface area of the S protein. This result may be due to the density of glycosylation on the S protein and is consistent with recent reports of a dominant G2-like class following MERS S-2P immunization in mice.[44] MERS-CoV S has ~22 *N*-linked glycans per monomer, 8 of which reside in the S1-NTD.[16] Previous work has demonstrated the ability of Abs to maneuver through the glycan shield. LCA60, a MERS-CoV RBD-specific mAb, accommodates nearby glycans, and G4, a MERS-CoV S2-specific Ab, avoids penetrating the glycan shield via its angle of approach.

We previously characterized the specificity and neutralizing activity of ~20 MERS-CoV S-specific mAbs that recognize the RBD, S1 NTD, and S2 regions.[45] RBD-specific mAbs tended to have potent neutralizing activity *in vitro*, suggesting that the RBD may be an effective vaccine target. For example, our RBD-specific CDC2-C2 human mAb has an IC_{50} pseudovirus neutralizing activity of 0.006 μg/mL and is nearly 10-fold more potent than our best NTD-specific mAb G2 [45]. In these studies, we showed that, despite similar levels of pseudovirus neutralizing activity, G2 protected mice against the MERS-CoV challenge whereas CDC2-C2 did not. These findings suggest that targets for neutralizing Abs outside the RBD may be underestimated. For example, mAb IgG22, isolated from mice vaccinated with a stabilized MERS S2 antigen, neutralized authentic MERS-CoV virus but not SARS-CoV-2 yet protected against both in challenge.[46] As such, protective antibody functionality will be important to consider as MERS-CoV vaccines are developed and may be relevant to ongoing COVID-19 vaccine development.

Compared with mAbs, polyclonal NTD- and RBD-depleted vaccine-induced IgG showed similar patterns of domain-specific pseudovirus neutralizing activity and protection. IgG derived from post-immunization sera depleted of NTD-specific Abs exhibited a substantial reduction in protective efficacy in MERS-CoV-infected mice. Further experiments are required to define protective thresholds for MERS-CoV S-2P vaccine-induced domain-specific polyclonal Abs in mice. Differences in relative neutralizing activity in RBD-depleted immune sera between pseudovirus and live-virus neutralization assays suggest that NTD-specific Ab neutralization may be affected by the density of S on the virion surface or other factors that distinguish S access on pseudoviruses from live MERS-CoV. Because pseudovirus neutralization explicitly measures the inhibition of viral entry mediated by S, other factors that may affect S access on pseudoviruses include by are not limited to the size of lentivirus-based pseudovirions or lack of malleability of the lentivirus backbone such that occluded S epitopes are difficult to access. Additionally, pseudovirus neutralization assays do not measure the inhibition of virus replication, cell-to-cell spread, or interactions with other viral surface proteins that are accounted for in a 4-day PRNT with live virus. Consistent with these findings, others have demonstrated that RBD-specific mAbs act by preventing DPP4 binding.[8,9,22,24] Interestingly, for SARS-CoV-2 vaccine-induced RBD-depleted serum and NTD-specific mAbs, pseudovirus neutralization is more robust in cell lines with less ACE2 receptor presence,[47] perhaps alluding to differences we see with the ability of RBD-depleted IgGs to neutralize MERS-CoV pseudoviruses and live viruses in Huh7.5 and Vero81 cells, respectively. Understanding the basis for the functional discordance of neutralizing and non-neutralizing NTD and non-RBD-directed mAbs against pseudovirus versus live virus may reveal new vulnerable targets on the spike protein that could inform the future development of vaccines against MERS-CoV and other CoVs, including SARS-CoV-2.

In summary, our work highlights the importance of eliciting Abs against antigenic domains outside of the RBD and illustrates the potential advantages of using the entire S ectodomain in the immunogen. Understanding how the requirements for *in vitro* neutralization differ from those required for *in vivo* protection will be essential for establishing correlates of immunity that can be interpreted across vaccine platforms.

Limitations of the study

There are limitations to our study that offer prospects for further investigation. Since our study involves immunization and the protective efficacy of domain-specific polyclonal responses elicited in vaccinated murine models, our results and interpretations depend on the limited; future studies will be needed to expand on findings in higher-order mammals, such as nonhuman primates and humans. A more thorough understanding of how MERS-CoV S-2P-induced NTD-specific antibody responses protect *in vivo*, such as assessments of Fc-mediated effector functions, is warranted. Finally, the designed full-length stabilized spike MERS S-2P_ΔRBD should be demonstrated on

other coronavirus spikes to demonstrate the broad generalizability of this approach and the relevance of NTD-specific protective antibody responses to other coronaviruses.

RESOURCE AVAILABILITY

Lead contact

Kizzmekia S. Corbett-Helaire (kizzmekia_corbett@hsph.harvard.edu).

Materials availability

Further information and requests for resources and reagents should be directed to and will be fulfilled by the lead contact.

Data and code availability

- Data: The negative-stain EM map of MERS spike ectodomain with NTD polyclonal antibodies have been deposited at the Electron Microscopy DataBank (EMDB) with accession code EMD-46715 (EMDB: EMD-46715).
- Code: N/A
- Other: All other datasets generated and/or analyzed in the current study are available from the corresponding author upon reasonable request.

ACKNOWLEDGMENTS

We thank members of the Vaccine Research Center (VRC) laboratories for their critical review of the article; Emily Phung and Tracy Ruckwardt for the preliminary optimization of foldon competition ELISA; Joan Ngwuta for the preliminary optimization of Ab depletion procedures; and Tracy Ruckwardt, Seyhan Boyoglu-Barnum, Geoffrey Hutchinson, and members of the VRC Translational Research Program for technical assistance with immunogenicity experiments; Nicole Doria-Rose for consultation regarding neutralization assays. This work was supported, in part, by The Vaccine Research Center, an intramural division of National Institute of Allergy and Infectious Diseases, National Institutes of Health. EM data collection and analyses were funded under NIH contract HHSN261200800001E (to A.B.W). PRNT assays were funded under NIH contract HHSN261200800001E Agreement 6x142 (to M.R.D. and J.D.C). MERS mouse challenge studies were funded under AI167966 and NIH Contract HHSN272201700036 Task Order No. 75N93019F00132 Requisition No. 5494549 (to R.S.B.). All contracts were furnished through Leidos Biomedical Research, Inc. K.S.C's research fellowship was partially funded by the Undergraduate Scholarship Program, Office of Intramural Training and Education, Office of the Director, National Institutes of Health. J.S.M. and A.B.W were supported by R01AI127521. The completion of this article was partially funded by K.S.C's start-up funds from Harvard T.H. Chan School of Public Health.

AUTHOR CONTRIBUTIONS

Conceptualization: K.S.C-H., B.S.G., N.W., and J.S.M. Methodology: K.S.C-H., O.M.A., N. W., S.R.L. A.S. A.C, L.W. S.B., L.J.S., R.L.G, J.F.K. Y.T., M.K., A.K., O.R., W.S., A.P.W., Y.Z., C.T.Z, and W-P.K.; visualization: K.S.C-H.,S.B., and N.W. C.P.; formal analysis: K.S.C-H., S.B., and Y.T.; supervision: K.S.C-H, J.R.M., A.B.W., M.R.D., J.D.C., R.B., J.S.M, and B.S.G, funding acquisition: K.S.C-H, J.R.M., A.B.W., M.R.D., J.D.C., R.B., J.S.M, and B.S.G; writing (original draft): K.S.C-H., B.S.G. K.M.M., O.M.A., C.K.O.D., and C.P.; writing (revision and editing): all authors.

DECLARATION OF INTERESTS

N.W., K.S.C-H, M.K., A.W., B.S.G., and J.S.M. are inventors on a US patent entitled "Prefusion Coronavirus Spike Proteins and Their Use." L.W., W.S., W.-P.K., M.K., J.R.M., and B.S.G. are inventors on a US patent application entitled "Middle East Respiratory Syndrome Coronavirus Immunogens, Antibodies, and Their Use."

STAR★METHODS

Detailed methods are provided in the online version of this paper and include the following:

- KEY RESOURCES TABLE
- EXPERIMENTAL MODELS AND STUDY PARTICIPANT DETAILS
  - Mouse models
  - Cell lines
  - MERS-CoV pseudoviruses
  - Live MERS-CoV
- METHOD DETAILS
  - Design and production of MERS S-2P_ΔRBD protein
  - Design and production of recombinant minifibritin foldon protein
  - Protein expression and purification
  - Antibody expression and purification
  - Negative-stain electron microscopy
  - MERS-CoV S domain-specific antibody depletion
  - ELISA
  - Pseudovirus neutralization assay
  - PRNTs
  - Electron microscopy-based polyclonal epitope mapping
- QUANTIFICATION AND STATISTICAL ANALYSES

SUPPLEMENTAL INFORMATION

Supplemental information can be found online at https://doi.org/10.1016/j.isci.2024.111632.

Received: September 3, 2024
Revised: October 31, 2024
Accepted: December 16, 2024
Published: December 18, 2024

REFERENCES

1. Fan, Y., Zhao, K., Shi, Z.L., and Zhou, P. (2019). Bat Coronaviruses in China. Viruses *11*, 210. https://doi.org/10.3390/v11030210.
2. Zumla, A., Peiris, M., Memish, Z.A., and Perlman, S. (2024). Anticipating a MERS-like coronavirus as a potential pandemic threat. Lancet *403*, 1729–1731. https://doi.org/10.1016/S0140-6736(24)00641-X.
3. Singh, S.K. (2016). Middle East Respiratory Syndrome Virus Pathogenesis. Semin. Respir. Crit. Care Med. *37*, 572–577. https://doi.org/10.1055/s-0036-1584796.
4. Widagdo, W., Sooksawasdi Na Ayudhya, S., Hundie, G.B., and Haagmans, B.L. (2019). Host Determinants of MERS-CoV Transmission and Pathogenesis. Viruses *11*, 280. https://doi.org/10.3390/v11030280.
5. Chen, Y., Lu, S., Jia, H., Deng, Y., Zhou, J., Huang, B., Yu, Y., Lan, J., Wang, W., Lou, Y., et al. (2017). A novel neutralizing monoclonal antibody targeting the N-terminal domain of the MERS-CoV spike protein. Emerg. Microb. Infect. *6*, e37. https://doi.org/10.1038/emi.2017.18.
6. Corti, D., Zhao, J., Pedotti, M., Simonelli, L., Agnihothram, S., Fett, C., Fernandez-Rodriguez, B., Foglierini, M., Agatic, G., Vanzetta, F., et al. (2015). Prophylactic and postexposure efficacy of a potent human monoclonal antibody against MERS coronavirus. Proc. Natl. Acad. Sci. USA *112*, 10473–10478. https://doi.org/10.1073/pnas.1510199112.
7. Johnson, R.F., Bagci, U., Keith, L., Tang, X., Mollura, D.J., Zeitlin, L., Qin, J., Huzella, L., Bartos, C.J., Bohorova, N., et al. (2016). 3B11-N, a monoclonal antibody against MERS-CoV, reduces lung pathology in rhesus monkeys following intratracheal inoculation of MERS-CoV Jordan-n3/2012. Virology *490*, 49–58. https://doi.org/10.1016/j.virol.2016.01.004.
8. Wang, L., Shi, W., Chappell, J.D., Joyce, M.G., Zhang, Y., Kanekiyo, M., Becker, M.M., van Doremalen, N., Fischer, R., Wang, N., et al. (2018). Importance of neutralizing monoclonal antibodies targeting multiple

antigenic sites on MERS-CoV Spike to avoid neutralization escape. J. Virol. *92*, e02002-17. https://doi.org/10.1128/jvi.02002-17.

9. Yu, X., Zhang, S., Jiang, L., Cui, Y., Li, D., Wang, D., Wang, N., Fu, L., Shi, X., Li, Z., et al. (2015). Structural basis for the neutralization of MERS-CoV by a human monoclonal antibody MERS-27. Sci. Rep. *5*, 13133. https://doi.org/10.1038/srep13133.
10. Zhou, Y., Yang, Y., Huang, J., Jiang, S., and Du, L. (2019). Advances in MERS-CoV Vaccines and Therapeutics Based on the Receptor-Binding Domain. Viruses *11*, 60. https://doi.org/10.3390/v11010060.
11. Baum, A., Fulton, B.O., Wloga, E., Copin, R., Pascal, K.E., Russo, V., Giordano, S., Lanza, K., Negron, N., Ni, M., et al. (2020). Antibody cocktail to SARS-CoV-2 spike protein prevents rapid mutational escape seen with individual antibodies. Science *369*, 1014–1018. https://doi.org/10.1126/science.abd0831.
12. Peng, Y., Mentzer, A.J., Liu, G., Yao, X., Yin, Z., Dong, D., Dejnirattisai, W., Rostron, T., Supasa, P., Liu, C., et al. (2020). Broad and strong memory $CD4^+$ and $CD8^+$ T cells induced by SARS-CoV-2 in UK convalescent COVID-19 patients. Preprint at bioRxiv. https://doi.org/10.1038/s41590-020-0782-6.
13. Raj, V.S., Mou, H., Smits, S.L., Dekkers, D.H.W., Müller, M.A., Dijkman, R., Muth, D., Demmers, J.A.A., Zaki, A., Fouchier, R.A.M., et al. (2013). Dipeptidyl peptidase 4 is a functional receptor for the emerging human coronavirus-EMC. Nature *495*, 251–254. https://doi.org/10.1038/nature12005.
14. Du, L., Zhao, G., Kou, Z., Ma, C., Sun, S., Poon, V.K.M., Lu, L., Wang, L., Debnath, A.K., Zheng, B.-J., et al. (2013). Identification of a Receptor-Binding Domain in the S Protein of the Novel Human Coronavirus Middle East Respiratory Syndrome Coronavirus as an Essential Target for Vaccine Development. J. Virol. *87*, 9939–9942. https://doi.org/10.1128/jvi.01048-13.
15. Wang, N., Shi, X., Jiang, L., Zhang, S., Wang, D., Tong, P., Guo, D., Fu, L., Cui, Y., Liu, X., et al. (2013). Structure of MERS-CoV spike receptor-binding domain complexed with human receptor DPP4. Cell Res. *23*, 986–993. https://doi.org/10.1038/cr.2013.92.
16. Yuan, Y., Cao, D., Zhang, Y., Ma, J., Qi, J., Wang, Q., Lu, G., Wu, Y., Yan, J., Shi, Y., et al. (2017). Cryo-EM structures of MERS-CoV and SARS-CoV spike glycoproteins reveal the dynamic receptor binding domains. Nat. Commun. *8*, 15092. https://doi.org/10.1038/ncomms15092.
17. Pallesen, J., Wang, N., Corbett, K.S., Wrapp, D., Kirchdoerfer, R.N., Turner, H.L., Cottrell, C.A., Becker, M.M., Wang, L., Shi, W., et al. (2017). Immunogenicity and structures of a rationally designed prefusion MERS-CoV spike antigen. Proc. Natl. Acad. Sci. USA *114*, E7348–E7357. https://doi.org/10.1073/pnas.1707304114.
18. Kirchdoerfer, R.N., Cottrell, C.A., Wang, N., Pallesen, J., Yassine, H.M., Turner, H.L., Corbett, K.S., Graham, B.S., McLellan, J.S., and Ward, A.B. (2016). Pre-fusion structure of a human coronavirus spike protein. Nature *531*, 118–121. https://doi.org/10.1038/nature17200.
19. Walls, A.C., Tortorici, M.A., Bosch, B.-J., Frenz, B., Rottier, P.J.M., DiMaio, F., Rey, F.A., and Veesler, D. (2016). Cryo-electron microscopy structure of a coronavirus spike glycoprotein trimer. Nature *531*, 114–117. https://doi.org/10.1038/nature16988.
20. Shang, J., Zheng, Y., Yang, Y., Liu, C., Geng, Q., Luo, C., Zhang, W., and Li, F. (2018). Cryo-EM structure of infectious bronchitis coronavirus spike protein reveals structural and functional evolution of coronavirus spike proteins. PLoS Pathog. *14*, e1007009. https://doi.org/10.1371/journal.ppat.1007009.
21. Wang, W., Wang, H., Deng, Y., Song, T., Lan, J., Wu, G., Ke, C., and Tan, W. (2016). Characterization of anti-MERS-CoV antibodies against various recombinant structural antigens of MERS-CoV in an imported case in China. Emerg. Microb. Infect. *5*, e113. https://doi.org/10.1038/emi.2016.114.
22. Wang, L., Shi, W., Joyce, M.G., Modjarrad, K., Zhang, Y., Leung, K., Lees, C.R., Zhou, T., Yassine, H.M., Kanekiyo, M., et al. (2015). Evaluation of candidate vaccine approaches for MERS-CoV. Nat. Commun. *6*, 7712. https://doi.org/10.1038/ncomms8712.
23. Kim, Y., Lee, H., Park, K., Park, S., Lim, J.H., So, M.K., Woo, H.M., Ko, H., Lee, J.M., Lim, S.H., et al. (2019). Selection and Characterization of Monoclonal Antibodies Targeting Middle East Respiratory Syndrome Coronavirus through a Human Synthetic Fab Phage Display Library Panning. Antibodies *8*, 42. https://doi.org/10.3390/antib8030042.
24. Widjaja, I., Wang, C., van Haperen, R., Gutiérrez-Álvarez, J., van Dieren, B., Okba, N.M.A., Raj, V.S., Li, W., Fernandez-Delgado, R., Grosveld, F., et al. (2019). Towards a solution to MERS: protective human monoclonal antibodies targeting different domains and functions of the MERS-coronavirus spike glycoprotein. Emerg. Microb. Infect. *8*, 516–530. https://doi.org/10.1080/22221751.2019.1597644.
25. Tse, L.V., Hou, Y.J., McFadden, E., Lee, R.E., Scobey, T.D., Leist, S.R., Martinez, D.R., Meganck, R.M., Schäfer, A., Yount, B.L., et al. (2023). A MERS-CoV antibody neutralizes a pre-emerging group 2c bat coronavirus. Sci. Transl. Med. *15*, eadg5567. https://doi.org/10.1126/scitranslmed.adg5567.
26. Zhou, H., Chen, Y., Zhang, S., Niu, P., Qin, K., Jia, W., Huang, B., Zhang, S., Lan, J., Zhang, L., et al. (2019). Structural definition of a neutralization epitope on the N-terminal domain of MERS-CoV spike glycoprotein. Nat. Commun. *10*, 3068. https://doi.org/10.1038/s41467-019-10897-4.
27. Wang, N., Rosen, O., Wang, L., Turner, H.L., Stevens, L.J., Corbett, K.S., Bowman, C.A., Pallesen, J., Shi, W., Zhang, Y., et al. (2019). Structural Definition of a Neutralization-Sensitive Epitope on the MERS-CoV S1-NTD. Cell Rep. *28*, 3395–3405. https://doi.org/10.1016/j.celrep.2019.08.052.
28. Dacon, C., Tucker, C., Peng, L., Lee, C.-C.D., Lin, T.-H., Yuan, M., Cong, Y., Wang, L., Purser, L., Williams, J.K., et al. (2022). Broadly neutralizing antibodies target the coronavirus fusion peptide. Science *377*, 728–735. https://doi.org/10.1126/science.abq3773.
29. Low, J.S., Jerak, J., Tortorici, M.A., McCallum, M., Pinto, D., Cassotta, A., Foglierini, M., Mele, F., Abdelnabi, R., Weynand, B., et al. (2022). ACE2-binding exposes the SARS-CoV-2 fusion peptide to broadly neutralizing coronavirus antibodies. Science *377*, 735–742. https://doi.org/10.1126/science.abq2679.
30. Zhou, P., Yuan, M., Song, G., Beutler, N., Shaabani, N., Huang, D., He, W.-T., Zhu, X., Callaghan, S., Yong, P., et al. (2022). A human antibody reveals a conserved site on beta-coronavirus spike proteins and confers protection against SARS-CoV-2 infection. Sci. Transl. Med. *14*, eabi9215. https://doi.org/10.1126/scitranslmed.abi9215.
31. Corbett, K.S., Edwards, D.K., Leist, S.R., Abiona, O.M., Boyoglu-Barnum, S., Gillespie, R.A., Himansu, S., Schäfer, A., Ziwawo, C.T., DiPiazza, A.T., et al. (2020). SARS-CoV-2 mRNA vaccine design enabled by prototype pathogen preparedness. Nature *586*, 567–571. https://doi.org/10.1038/s41586-020-2622-0.
32. Tian, J.-H., Patel, N., Haupt, R., Zhou, H., Weston, S., Hammond, H., Logue, J., Portnoff, A.D., Norton, J., Guebre-Xabier, M., et al. (2021). SARS-CoV-2 spike glycoprotein vaccine candidate NVX-CoV2373 immunogenicity in baboons and protection in mice. Nat. Commun. *12*, 372. https://doi.org/10.1038/s41467-020-20653-8.
33. Sahin, U., Muik, A., Vogler, I., Derhovanessian, E., Kranz, L.M., Vormehr, M., Quandt, J., Bidmon, N., Ulges, A., Baum, A., et al. (2021). BNT162b2 vaccine induces neutralizing antibodies and poly-specific T cells in humans. Nature *595*, 572–577. https://doi.org/10.1038/s41586-021-03653-6.
34. Cockrell, A.S., Yount, B.L., Scobey, T., Jensen, K., Douglas, M., Beall, A., Tang, X.C., Marasco, W.A., Heise, M.T., and Baric, R.S. (2016). A mouse model for MERS coronavirus-induced acute respiratory distress syndrome. Nat. Microbiol. *2*, 16226. https://doi.org/10.1038/nmicrobiol.2016.226.
35. Leist, S.R., Jensen, K.L., Baric, R.S., and Sheahan, T.P. (2019). Increasing the translation of mouse models of MERS coronavirus pathogenesis through kinetic hematological analysis. PLoS One *14*, e0220126. https://doi.org/10.1371/journal.pone.0220126.

36. Adams, L.E., Leist, S.R., Dinnon, K.H., 3rd, West, A., Gully, K.L., Anderson, E.J., Loome, J.F., Madden, E.A., Powers, J.M., Schäfer, A., et al. (2023). Fc-mediated pan-sarbecovirus protection after alphavirus vector vaccination. Cell Rep. *42*, 112326. https://doi.org/10.1016/j.celrep.2023.112326.

37. Mackin, S.R., Desai, P., Whitener, B.M., Karl, C.E., Liu, M., Baric, R.S., Edwards, D.K., Chicz, T.M., McNamara, R.P., Alter, G., and Diamond, M.S. (2023). Fc-γR-dependent antibody effector functions are required for vaccine-mediated protection against antigen-shifted variants of SARS-CoV-2. Nat. Microbiol. *8*, 569–580. https://doi.org/10.1038/s41564-023-01359-1.

38. Dagotto, G., Ventura, J.D., Martinez, D.R., Anioke, T., Chung, B.S., Siamatu, M., Barrett, J., Miller, J., Schäfer, A., Yu, J., et al. (2022). Immunogenicity and protective efficacy of a rhesus adenoviral vaccine targeting conserved COVID-19 replication transcription complex. NPJ Vaccines *7*, 125. https://doi.org/10.1038/s41541-022-00553-2.

39. Kingstad-Bakke, B., Cleven, T., Bussan, H., Yount, B.L., Jr., Uraki, R., Iwatsuki-Horimoto, K., Koga, M., Yamamoto, S., Yotsuyanagi, H., Park, H., et al. (2023). Airway surveillance and lung viral control by memory T cells induced by COVID-19 mRNA vaccine. JCI Insight *8*, e172510. https://doi.org/10.1172/jci.insight.172510.

40. Wang, L., Shi, W., Chappell, J.D., Joyce, M.G., Zhang, Y., Kanekiyo, M., Becker, M.M., van Doremalen, N., Fischer, R., Wang, N., et al. (2018). Importance of Neutralizing Monoclonal Antibodies Targeting Multiple Antigenic Sites on the Middle East Respiratory Syndrome Coronavirus Spike Glycoprotein To Avoid Neutralization Escape. J. Virol. *92*, 10–128. https://doi.org/10.1128/JVI.02002-17.

41. (2024). Pathogens prioritization: a scientific framework for epidemic and pandemic research preparedness. https://cdn.who.int/media/docs/default-source/consultation-rdb/prioritization-pathogens-v6final.pdf?sfvrsn=c98effa7_7&download=true.

42. Musunuri, S., Weidenbacher, P.A.B., and Kim, P.S. (2024). Bringing immunofocusing into focus. npj Vaccines *9*, 11. https://doi.org/10.1038/s41541-023-00792-x.

43. Chao, C.W., Sprouse, K.R., Miranda, M.C., Catanzaro, N.J., Hubbard, M.L., Addetia, A., Stewart, C., Brown, J.T., Dosey, A., Valdez, A., et al. (2024). Protein nanoparticle vaccines induce potent neutralizing antibody responses against MERS-CoV. Preprint at bioRxiv. https://doi.org/10.1101/2024.03.13.584735.

44. Addetia, A., Stewart, C., Seo, A.J., Sprouse, K.R., Asiri, A.Y., Al-Mozaini, M., Memish, Z.A., Alshukairi, A.N., and Veesler, D. (2024). Mapping immunodominant sites on the MERS-CoV spike glycoprotein targeted by infection-elicited antibodies in humans. Cell Rep. *43*, 114530. https://doi.org/10.1016/j.celrep.2024.114530.

45. Choi, J.-H., Woo, H.-M., Lee, T.-Y., Lee, S.-Y., Shim, S.-M., Park, W.-J., Yang, J.-S., Kim, J.A., Yun, M.-R., Kim, D.-W., et al. (2020). Characterization of a human monoclonal antibody generated from a B-cell specific for a prefusion-stabilized spike protein of Middle East respiratory syndrome coronavirus. PLoS One *15*, e0232757. https://doi.org/10.1371/journal.pone.0232757.

46. Hsieh, C.L., Werner, A.P., Leist, S.R., Stevens, L.J., Falconer, E., Goldsmith, J.A., Chou, C.W., Abiona, O.M., West, A., Westendorf, K., et al. (2021). Stabilized coronavirus spike stem elicits a broadly protective antibody. Cell Rep. *37*, 109929. https://doi.org/10.1016/j.celrep.2021.109929.

47. Farrell, A.G., Dadonaite, B., Greaney, A.J., Eguia, R., Loes, A.N., Franko, N.M., Logue, J., Carreño, J.M., Abbad, A., Chu, H.Y., et al. (2022). Receptor-Binding Domain (RBD) Antibodies Contribute More to SARS-CoV-2 Neutralization When Target Cells Express High Levels of ACE2. Viruses *14*, 2061.

48. Beeler, J.A., and van Wyke Coelingh, K. (1989). Neutralization epitopes of the F glycoprotein of respiratory syncytial virus: effect of mutation upon fusion function. J. Virol. *63*, 2941–2950. https://doi.org/10.1128/jvi.63.7.2941-2950.1989.

49. Douglas, M.G., Kocher, J.F., Scobey, T., Baric, R.S., and Cockrell, A.S. (2018). Adaptive evolution influences the infectious dose of MERS-CoV necessary to achieve severe respiratory disease. Virology *517*, 98–107. https://doi.org/10.1016/j.virol.2017.12.006.

50. Almazán, F., DeDiego, M.L., Sola, I., Zuñiga, S., Nieto-Torres, J.L., Marquez-Jurado, S., Andrés, G., and Enjuanes, L. (2013). Engineering a Replication-Competent, Propagation-Defective Middle East Respiratory Syndrome Coronavirus as a Vaccine Candidate. mBio *4*, e00650-13. https://doi.org/10.1128/mBio.00650-13.

51. Scobey, T., Yount, B.L., Sims, A.C., Donaldson, E.F., Agnihothram, S.S., Menachery, V.D., Graham, R.L., Swanstrom, J., Bove, P.F., Kim, J.D., et al. (2013). Reverse genetics with a full-length infectious cDNA of the Middle East respiratory syndrome coronavirus. Proc. Natl. Acad. Sci. USA *110*, 16157–16162. https://doi.org/10.1073/pnas.1311542110.

52. McLellan, J.S., Chen, M., Joyce, M.G., Sastry, M., Stewart-Jones, G.B.E., Yang, Y., Zhang, B., Chen, L., Srivatsan, S., Zheng, A., et al. (2013). Structure-based design of a fusion glycoprotein vaccine for respiratory syncytial virus. Science *342*, 592–598. https://doi.org/10.1126/science.1243283.

53. Leist, S.R., and Cockrell, A.S. (2020). Genetically Engineering a Susceptible Mouse Model for MERS-CoV-Induced Acute Respiratory Distress Syndrome. Methods Mol Biol *2099*, 137–159. https://doi.org/10.1007/978-1-0716-0211-9_12.

54. Stewart, S.A., Dykxhoorn, D.M., Palliser, D., Mizuno, H., Yu, E.Y., An, D.S., Sabatini, D.M., Chen, I.S., Hahn, W.C., Sharp, P.A., et al. (2003). Lentivirus-delivered stable gene silencing by RNAi in primary cells. RNA *9*, 493–501.

55. Pettersen, E.F., Goddard, T.D., Huang, C.C., Couch, G.S., Greenblatt, D.M., Meng, E.C., and Ferrin, T.E. (2004). UCSF Chimera–a visualization system for exploratory research and analysis. J. Comput. Chem. *25*, 1605–1612.

56. Potter, C.S., Chu, H., Frey, B., Green, C., Kisseberth, N., Madden, T.J., Miller, K.L., Nahrstedt, K., Pulokas, J., Reilein, A., et al. (1999). Leginon: a system for fully automated acquisition of 1000 electron micrographs a day. Ultramicroscopy *77*, 153–161.

57. Lander, G.C., Stagg, S.M., Voss, N.R., Cheng, A., Fellmann, D., Pulokas, J., Yoshioka, C., Irving, C., Mulder, A., Lau, P.W., et al. (2009). Appion: an integrated, database-driven pipeline to facilitate EM image processing. J. Struct. Biol. *166*, 95–102.

58. Kimanius, D., Forsberg, B.O., Scheres, S.H., and Lindahl, E. (2016). Accelerated cryo-EM structure determination with parallelisation using GPUs in RELION-2. elife *5*, e18722.

59. Cockrell, A.S., Yount, B.L., Scobey, T., Jensen, K., Douglas, M., Beall, A., Tang, X.-C., Marasco, W.A., Heise, M.T., and Baric, R.S. (2016). A mouse model for MERS coronavirus-induced acute respiratory distress syndrome. Nat. Microbiol. *2*, 16226. https://doi.org/10.1038/nmicrobiol.2016.226.

60. Bianchi, M., Turner, H.L., Nogal, B., Cottrell, C.A., Oyen, D., Pauthner, M., Bastidas, R., Nedellec, R., McCoy, L.E., Wilson, I.A., et al. (2018). Electron-Microscopy-Based Epitope Mapping Defines Specificities of Polyclonal Antibodies Elicited during HIV-1 BG505 Envelope Trimer Immunization. Immunity *49*, 288–300. https://doi.org/10.1016/j.immuni.2018.07.009.

61. Voss, N.R., Yoshioka, C.K., Radermacher, M., Potter, C.S., and Carragher, B. (2009). DoG Picker and TiltPicker: software tools to facilitate particle selection in single particle electron microscopy. J. Struct. Biol. *166*, 205–213.

STAR★METHODS

KEY RESOURCES TABLE

REAGENT or RESOURCE	SOURCE	IDENTIFIER
Antibodies		
Anti-MERS-CoV S antibody, G2	Wang et al.[8]	N/A
Anti-MERS-CoV S antibody, CDC2-A2	Wang et al.[8]	N/A
Anti-MERS-CoV S antibody, G4	Wang et al.[8]	N/A
Anti-MERS-CoV S antibody, D12	Wang et al.[8]	N/A
Anti-MERS-CoV S antibody, F11	Wang et al.[8]	N/A
Anti-MERS-CoV S antibody, CDC-C2	Wang et al.[8]	N/A
Anti-RSV glycoprotein F antibody, 1129	Beeler and van Wyke Coelingh[48]	N/A
Goat anti-mouse IgG-horseradish peroxidase (HRP) conjugate	Sigma-Aldrich	Cat # G-21040; RRID:AB_2536527
Goat anti-Human IgG (H+L) IgG horseradish peroxidase (HRP) conjugate	ThermoFisher Scientific	Cat #: A18811; RRID:AB_2535588
Bacterial and virus strains		
Mouse-adapted MERS-CoV EMC derivative, M35c4	Douglas et al.[49]	N/A
MERS-CoV EMC/2012	Almazán et al.[50] and Scobey et al.[51]	N/A
DH5a competent cells	ThermoFisher	Cat# 18258012
Chemicals, peptides, and recombinant proteins		
3,5,305'-tetramethylbenzidine (TMB)	KPL SureBlue	Cat# 5150-0021
Kifunensine	GlycoSyn	Cat# FC-034
25 kDa linear polyethyleneimine	Polysciences	Cat# 3966-2
ExpiFectamine 293 transfection reagent	ThermoFisher Scientific	Cat# A14525
Imidazole	ThermoFisher Scientific	Cat# AC122020050
FreeStyle 293 Expression Medium	GIBCO	Cat# 12338002
Expi293 Expression Medium	GIBCO	Cat# A1435101
OPTI-MEM, Reduced Serum Medium	ThermoFisher Scientific	Cat# 11058021
PBS	ThermoFisher Scientific	Cat# 10010023
Tris	Sigma-Aldrich	Cat# GE17-1321-01
QIAGEN Plasmid Maxi Kit	QIAGEN	Cat# 12162
Ampicillin sodium salt	Sigma-Aldrich	Cat# A9518
Kanamycin Sulfate	Sigma-Aldrich	Cat# K1876
Sodium Chloride	Sigma-Aldrich	Cat# S9888-1KG
D-desthiobiotin	MilliporeSigma	Cat#71610
Penicillin-Streptomycin	ThermoFisher Scientific	Cat#10378016
Fetal Bovine Serum (FBS)	ThermoFisher Scientific	Cat#10500064
10× Buffer E: Strep-Tactin Elution buffer with D-desthiobiotin	IBA Lifesciences	Cat# 2-1000
10× Buffer R; Strep-Tactin regeneration buffer with HABA	IBA Lifesciences	Cat# 2-1002
10× Buffer W: Strep-Tactin Wash buffer	IBA Lifesciences	Cat# 2-1003
T4 Minifibritin foldon protein	Pallesen et al.[17]	N/A
MERS NTD protein	Wang et al.[27]	N/A
MERS S1 protein	Wang et al.[22]	N/A
MERS RBD protein	Wang et al.[22]	N/A
MERS-CoV S-2P protein	Pallesen et al.[17]	N/A

(*Continued on next page*)

Continued

REAGENT or RESOURCE	SOURCE	IDENTIFIER
MERS-CoV S-2P ΔRBD protein	This manuscript	N/A
MERS S2_hFc protein	Wang et al.[22]	N/A
RSV pre-F	McLellan et al.[52]	N/A
Critical commercial assays		
Luciferase Assay System	Promega	Cat# E1500
Culture Lysis 5X Reagent	Promega	Cat# E1531
FuGENE HD Transfection Reagent	Promega	Cat# E2311
Deposited data		
EM map of Fabs CDC-A2 + MERS-CoV S-2P	This manuscript	EMDB ID :46715
Experimental models: Cell lines		
Expi293F Suspension Cells	ThermoFisher Scientific	Cat# A14527
293T cells	ATCC	Cat# CRL-11268
HEK293T/17	ATCC	Cat# CRL-11268
FreeStyle 293-F Cells	ThermoFisher Scientific	Cat# R79007
Vero 81 cells	ATCC	Cat# CCL-81
Huh7.5 cells	Provided by Dr. Deborah R. Taylor of the US FDA	N/A
Experimental models: Organisms/strains		
Mus musculus, strain C57BL/6J	Jackson Laboratories	JAX stock #000664
Mus musculus, strain 288/330+/+	Leist et al.[53]	N/A
Recombinant DNA		
pCMVDR8.2	Stewart et al.[54]	Addgene Cat#8455
pHR' CMV-Luc	Barney Graham Laboratory	N/A
CMV/R-MERS-CoV S	Barney Graham Laboratory	N/A
CMV/R-MERS-CoV maM35c4 S	Barney Graham Laboratory	N/A
paH expression plasmid	Jason McLellan Laboratory	N/A
pVRC8400 expression plasmid	Barney Graham Laboratory	N/A
pLEXm expression plasmid	Barney Graham Laboratory	N/A
paH-MERS S-WT-FL	Barney Graham Laboratory	N/A
paH-MERS S-WT	Barney Graham Laboratory	N/A
paH-MERS S1- 3CH2S	Barney Graham Laboratory	N/A
paH-MERS-CoV S-2P	Pallesen et al.[17]	N/A
paH-DPP4	Barney Graham Laboratory	N/A
paH-MERS-CoV S-2P ΔRBD	This manuscript	N/A
pαH MERS NTD-3CH2S	Barney Graham Laboratory	N/A
pαH MERS RBD-3C-HIS	Barney Graham Laboratory	N/A
Software and algorithms		
Prism (Version 9.2.0)	GraphPad	https://www.graphpad.com/
FlowJo (V10.4.1)	FlowJo	https://www.flowjo.com/
UCSF Chimera	Pettersen et al.[55]	RRID: SCR_004097
Leginon software suite	Potter et al.[56]	RRID: SCR_016731
Appion	Lander et al.[57]	RRID: SCR_016734
Relion 3.0	Kimanius et al.[58]	N/A
Other		
1N sulfuric acid	ThermoFisher	Cat# SA212-1
96-well Nunc MaxiSorp flat-bottom plates	ThermoFisher	Cat # 44-2401-21
PBS-T, PBS + 0.05% Tween 20	Medicago	Article # 09-9410-100
Difco skim milk (BD	BD	Cat# 232100

(*Continued on next page*)

Continued

REAGENT or RESOURCE	SOURCE	IDENTIFIER
Papain-agarose resin	ThermoFisher Scientific	Cat# 20341
Sigma Adjuvant System	Sigma-Aldrich	Cat# S6322-1VL
HRV3C protease	ThermoFisher Scientific	Cat# 88947
Pierce Protein G Agarose	ThermoFisher Scientific	Cat# 20398
Strep-Tactin Superflow resin	IBA Lifesciences	Cat# 2-1206-010
Pierce Protein A agarose	ThermoFisher Scientific	Cat# 20334
Ni NTA resin	QIAGEN	Cat# 88221
Superose 6 Increase 10/300 GL	GE Healthcare	Cat# 29091596
Superdex 200 10/300 GL	GE Healthcare	Cat# 28-9909-44
Super AquaBlue substrate	eBioscience	Cat# 00-4203-56
Carbon-coated 400-mesh Cu grids	Electron Microscopy Sciences	Cat# CF400-Cu-50
Dynamag-2	ThermoFisher Scientific	Cat# 12321D
Filter paper	Cytiva	Cat# 1004047
Empty Disposable Gravity Flow Columns, Fritted, 30 mL, with 20 μm frits	Malvergent Bioscience	Cat# 11-0260-025

EXPERIMENTAL MODELS AND STUDY PARTICIPANT DETAILS

Mouse models

Animal experiments were carried out in compliance with all pertinent US National Institutes of Health regulations and approval from the Animal Care and Use Committee of the Vaccine Research Center or University of North Carolina at Chapel Hill. For all vaccine studies, we adjuvanted immunogens with Sigma Adjuvant System, and we inoculated mice intramuscularly, as previously detailed.[17] To generate polyclonal Middle East respiratory syndrome (MERS) S-2P-immune IgG, we immunized 6- to 8-week-old female C57BL/6J mice (Jackson Laboratory) with 1 μg MERS S-2P protein at 0 and 3 weeks. Sera were collected at 2, 4, and 6 (terminal) weeks post-boost, pooled, and subjected to IgG purification with protein G (Life Technologies), per the manufacturer's protocol. For challenge studies to evaluate vaccines, we immunized 16- to 20-week-old 288/330$^{+/+}$ male and female mice[59] with a 0.02-μg molecular equivalent dose of MERS S1, MERS S-2P, or MERS S-2P_ΔRBD at 0 and 4 weeks. At 4 weeks post-boost, we collected pre-challenge sera from a subset of mice and challenged the remaining mice.

To evaluate the immunogenicity of passively transferred monoclonal antibodies (mAbs), we intraperitoneally (IP) immunized 20- to 25-week-old 288/330$^{+/+}$ male and female mice with 1 or 0.2 mg/kg of mAbs. We collected sera from a subset of mice at 11 h post-immunization and challenged the remaining mice at hour 12, when applicable. Similarly, for polyclonal IgG, we IP immunized 288/330$^{+/+}$ mice with 0.5 mg diluted in 0.5 mL of 1X phosphate-buffered saline (PBS). At hour 23, we collected a subset of sera, and at hour 24, we challenged the remaining mice. We completed all challenges with 5×10^5 PFU of a mouse-adapted MERS coronavirus (CoV) EMC derivative, M35c4 [49]. On day 3 and day 5, 6, or 7 post-challenge, lungs were harvested, and hemorrhaging and viral titers were assessed, per previously published methods.[51] In select mice, we also measured PenH (enhanced pause), a unitless measure that reflects airway obstruction/restriction due to debris in the airway, and EF50 (mid-tidal expiratory flow), which represents the flow rate at which 50% of the tidal volume has been expelled in a single breath.[59]

Cell lines

We cultured HEK293T/17 (American Type Culture Collection [ATCC], RRID:CVCL_1926) and Huh7.5 cells (provided by Deborah R. Taylor, US Food and Drug Administration, RRID:CVCL_7927) in Dulbecco's modified Eagle's medium (DMEM) supplemented with 10% fetal bovine serum (FBS), 2 mM glutamine, and 1% penicillin/streptomycin at 37°C and 5% CO_2. Vero 81 cells (ATCC Cat# CCL-81, RRID:CVCL_0059) used for PRNT assays were carried in DMEM supplemented with 10% FBS, 0.25 mg/ml amphotericin B, 100 units penicillin per ml, and 0.1 mg streptomycin per ml. DMEM used for PRNT agar overlays contained final concentrations of 12.5% FBS, 0.25 mg/ml mM amphotericin B, and 100 units penicillin per ml, 0.1 mg streptomycin per ml, and 1% agar. Cell lines were not authenticated or mycoplasma tested.

MERS-CoV pseudoviruses

We introduced divergent amino acids, as predicted from translated sequences, into the MERS-CoV EMC S gene (GenBank: AFS88936) to generate the MERS-CoV M35c4 S gene.[49] Subsequently, we produced MERS-CoV EMC and m35c4 pseudoviruses by co-transfection of plasmids encoding a luciferase reporter, lentivirus backbone, and spike genes in 293T cells, as previously described.[22]

Live MERS-CoV

For plaque reduction neutralization tests (PRNTs) with sera and IgG, we recovered the MERS-CoV EMC strain from a bacterial artificial chromosome containing the full-length viral genome, per previously published methods.[50]

METHOD DETAILS

Design and production of MERS S-2P_ΔRBD protein

Following methods similar to those for the design and production of MERS S-2P,[17] we synthesized a mammalian codon-optimized gene encoding MERS-CoV S (England1 strain) residues 1–1291, with a GSGG linker to connect Gly380 and Lys577, a C-terminal T4 fibritin trimerization domain, an HRV3C cleavage site, an 8x His-tag, and a Twin-Strep-tag; we then subcloned this gene into the eukaryotic expression vector pαH. The S1/S2 furin-recognition site 748-RSVR-751 was mutated to ASVG to produce a single-chain S0 protein. The construct was expressed by transient transfection of Expi293 cells (ThermoFisher Scientific) in suspension at 37°C for 6 days. We purified the protein from the supernatant using Strep-Tactin resin (IBA). We added HRV3C protease (1% wt/wt) to the protein and incubated the reaction overnight at 4°C to cleave the His-tag for usability in mouse inoculations. We further purified the digested protein using a Superose 6 Increase column (GE Healthcare).

Design and production of recombinant minifibritin foldon protein

We synthesized a mammalian codon-optimized plasmid encoding foldon-inserted minifibritin (ADIVLNDLPFVDGPPAEGQSRIS WIKNGEEILGADTQYGSEGSMNRPTVSVLRNVEVLDKNIGILKTSLETANSDIKTIQEAGYIPEAPRDGQAYVRKDGEWVLLSTFLSPALV PRGSHHHHHHSAWSHPQFEK) with a C-terminal thrombin cleavage site, a 6x His-tag, and Strep-tag II, which we then subcloned into a mammalian expression vector derived from pLEXm. The construct was expressed by transient transfection of Expi293 cells (ThermoFisher Scientific) in suspension at 37°C for 6 days. We first purified the protein with a Ni^{2+}-nitrilotriacetic acid (NTA) resin (GE Healthcare), using an elution buffer consisting of 50 mM Tris-HCl, pH 7.5, 400 mM NaCl, and 300 mM imidazole, pH 8.0. We further purified the protein with Strep-Tactin resin according to the manufacturer's instructions (IBA Lifesciences).

Protein expression and purification

Vectors encoding genes for foldon and MERS S-2P ΔRBD were expressed and purified as described above. We generated vectors encoding respiratory syncytial virus fusion protein (RSV pre-F),[52] MERS S-2P,[17] MERS NTD,[27] MERS S1, MERS RBD, and MERS S2_hFc[22] as previously described with the following small amendments. We induced protein expression by transfection of plasmids into Expi293 cells using Expifectamine transfection reagent (ThermoFisher Scientific) in suspension at 37°C for 6 days. We collected the transfected cell culture supernatants and purified the protein using Strep-Tactin resin (IBA) or NTA resin (GE Healthcare) when applicable. For proteins used in mouse inoculations, His-tags were cleaved by the addition of HRV3C protease (ThermoFisher Scientific) (1% wt/wt) overnight at 4°C. Size exclusion chromatography via a Superose 6 Increase column (GE Healthcare) yielded the final purified protein.

Antibody expression and purification

For mAbs, 1129,[48] CDC2-C2, CDC2-A2 [8], D12, G2, G4 [22], and paired heavy- and light-chain complementary DNA sequences were expressed in Expi293 cells and purified via protein A Fast Flow and Superdex column filtration (GE Healthcare), as previously detailed.

Negative-stain electron microscopy

The protein sample was diluted to 0.2 mg/ml with buffer containing 10 mM HEPES, pH 7, and 150 mM NaCl and adsorbed to a carbon-coated copper grid for 15 seconds. The grid was washed three times with the same buffer, followed by negative staining with 0.7% uranyl formate. Data was collected on a ThermoFisher Talos F200C electron microscope operated at 200 kV and equipped with a 4k × 4k Ceta camera at a nominal magnification of 57,000 corresponding to a pixel size of 0.25 nm. Reference-free 2D classification was performed using Relion.[44]

MERS-CoV S domain-specific antibody depletion

Heat-inactivated (HI) sera from vaccinated mice were diluted 1:100 and mixed with 25 μg/mL of the following His-tagged proteins: RSV pre-F,[52] which was used for mock depletion, MERS S-2P, MERS S1, MERS NTD, and MERS RBD. Similarly, we mixed polyclonal MERS S-2P-immune IgG with His-tagged proteins at a 1:2.5 IgG:protein ratio. We incubated the serum/IgG + protein mixtures for 1 h at room temperature (RT). Dynobeads for His-tag pulldown (ThermoFisher Scientific) were washed twice with 1X PBS and then added to the serum/IgG + protein mixture for 30 min at RT. Using Dynamag-2 (ThermoFisher Scientific) to capture protein-bound Abs, we analyzed supernatants containing domain-depleted Abs in subsequent immunoassays.

ELISA

We coated Nunc Maxisorp ELISA plates (ThermoFisher Scientific) with 100 ng of protein in PBS at 4°C overnight or for 2 h at RT. When applicable, to eliminate foldon-specific binding from MERS S-2P- or MERS S-2P_ ΔRBD immunized with serial dilutions of mouse

serum or purified IgG, we added 50 μg/mL of foldon protein for 1 h at RT. After standard washes and blocks, we incubated plates with sera, purified IgG, or mAbs for 1 h at RT. Anti-mouse IgG1 or IgG2a-horseradish peroxidase (HRP) conjugates (Jackson Laboratory) were used as secondary Abs, and 3,5,3′5′-tetramethylbenzidine (TMB) (KPL) was used as the substrate to detect Ab responses. We calculated end-point titers as the dilution that emitted an optical density (OD) exceeding a level of four times the background (secondary Ab autofluorescence). We performed kinetic ELISAs as mentioned previously; however, we used Super AquaBlue substrate (eBioscience) as the substrate to detect Ab responses, and we read the rate of color change in mOD/min at a wavelength of 405 nm every 9 s for 5 min. We completed the competition ELISA using 250 ng/well of recombinant MERS S1 protein. Following standard washes and blocks, dilutions of domain-depleted IgG were incubated in wells for 15 min at RT, followed by the addition of optimized amounts of biotinylated mAb for 1 h at RT. We utilized secondary Ab streptavidin HRP (ThermoFisher Scientific) TMB (KPL) to detect the amount of bound biotinylated Ab. The standard curve was optimized for each individual mAb and used as an experimental control.

Pseudovirus neutralization assay

Pseudovirus neutralization assay methods have been previously described.[17] Briefly, HI serum, purified IgG, or mAbs were mixed with MERS-CoV EMC or M35c4 pseudoviruses, incubated, and then added to Huh 7.5 cells. After 72 h, we lysed the cells and measured the relative luciferase activity. We calculated the percent neutralization, considering uninfected cells as 100% neutralization and cells transduced with only pseudovirus as 0% neutralization. We determined IC_{50} titers based on sigmoidal nonlinear regression.

PRNTs

MERS-CoV EMC strain recovered from a bacterial artificial chromosome containing the full-length viral genome[50] was subjected to a PRNT with serial $\log_4$ dilutions of purified IgG (starting at 100 μg/mL) or HI sera (starting at 1:6). Vero 81 cells were seeded in 6-well plates at $1x10^6$ cells per well and allowed to reach confluence within 24h. We mixed IgG or sera with 3.2×10^1–1.40×10^2 PFU of MERS-CoV in a total volume of 200 μL gelatin saline (0.3% [wt/vol] gelatin in 1X PBS supplemented with $CaCl_2$ and $MgCl_2$). Ab + virus mixtures were incubated for 20 min at 37°C, followed by adsorption of 100-μL aliquots to each of two confluent wells of Vero 81 cells in 6-well (10-cm^2) plates for 30 min at 37°C/5% CO_2. Monolayers were overlaid with DMEM containing 1% agar, and plates were incubated at 37°C/5% CO_2; plaques were enumerated at 4 days post-infection. We calculated the percent neutralization as the average number of plaques produced by IgG- or serum-treated virus divided by average number of plaques produced by virus in diluent alone.

Electron microscopy-based polyclonal epitope mapping

Polyclonal sample processing as described previously.[60] For Fab preparation, we buffer-exchanged 2 mg of polyclonal IgG samples into the digestion buffer (20 mM sodium phosphate + 10 mM ethylenediaminetetraacetic acid + 20 mM cysteine, pH 7.4) and incubated the samples with 250 μL of settled papain-agarose resin (ThermoFisher Scientific) at 37°C for 14 h. Undigested IgG were removed by size exclusion chromatography (Superose 6 Increase column) in PBS buffer, and we concentrated the fractions containing Fab via 10-kDa cutoff Amicon ultrafiltration units. Next, 200 μg of the Fab mixture was complexed with 20 μg of MERS S-2P protein and incubated for ~16 h at RT before size exclusion chromatography purification with Tris-buffered saline as the running buffer. The complexes were concentrated with 10-kDa cutoff Amicon ultrafiltration units, immediately loaded onto carbon-coated 400-mesh Cu grids and stained with 2% (w/v) uranyl-formate for 90 s immediately following sample application. Micrographs were collected on a 120-kv Tecnai Spirit microscope with a 4k×4k TemCam F416 camera using Leginon.[56] Particle picking[61] and stack creation was performed on Appion,[57] with further processing by Relion 3.0 (5) to obtain 2D class averages and three-dimensional (3D) classification. A subset of 3D classes with good Fab reconstructions was auto-refined on Relion 3.0 and used for producing composite figures via UCSF Chimera.

QUANTIFICATION AND STATISTICAL ANALYSES

In box plots, boxes and horizontal bars denote the interquartile range and median, which represent data outside the 25^{th}–75^{th} percentile range. Whisker endpoints indicate the minimum and maximum values. Geometric or arithmetic means are represented by the heights of bars or symbols, and error bars represent the corresponding standard deviation. Dotted lines indicate the assay limits of detection. Figure legends detail all quantification and statistical analyses, including animal numbers (n), dispersion and precision measures, and statistical tests performed. To compare more than two experimental groups, we applied the Kruskal–Wallis analysis of variance with Dunn's multiple-comparisons tests assuming a non-Gaussian distribution. We transformed reciprocal endpoint and reciprocal IC_{50} titers so that all values were on a $\log_{10}$ scale prior to statistical analyses. We performed statistical analyses using GraphPad Prism v9.2.0. Significance is denoted by asterisks defined as $^*P < 0.05$, $^{**}P < 0.01$, $^{***}P < 0.001$, $^{****}P < 0.0001$.